

Effect of Stirring and Lanthanum in the Steel on the Interfacial Reaction Between the Steel and the MgO-C Refractory



Mingzhe Zhao and Lifeng Zhang

Abstract In the current study, laboratory experiments were performed to investigate the interfacial reaction between the molten steel and the MgO-C refractory, and the effect of lanthanum in the steel was studied. A dense MgO reaction layer with a 50 μm thickness at the interface between the quiescent steel without lanthanum and the refractory was observed. Under stirring condition, the thickness of the MgO reaction layer was only 25 μm and the layer was non-continuous and broken at some places. For the interfacial interaction between the lanthanum-bearing steel and the MgO-C refractory, under quiescent condition, a double-layer structure was generated, with a MgO layer close to the refractory side and a La_2O_3 layer close to the steel side. Under stirring condition, a La_2O_3 - $\text{La}_2\text{O}_2\text{S}$ layer was generated and a few LaAlO_3 particles were embedded inside the MgO reaction layer. The stirring induced the dislodgement of MgO particles from the lining refractory into the molten steel.

Keywords Interfacial reaction · Lanthanum-bearing steel · MgO-C refractory

Introduction

During the steelmaking process, the refractory material is in direct contact with molten steel. The chemical corrosion and physical scouring of molten steel on the refractory material are inevitable, which significantly reduces the service life of the ladle lining. This limitation affects the steel quality and smelting safety [1]. It is well known that the addition of rare earth elements can modify the inclusions in steel and improve its mechanical properties [2–5]. However, due to their strong

M. Zhao

School of Materials Science and Engineering, Yanshan University, Qinhuangdao 066004, China

L. Zhang (✉)

School of Mechanical and Material Engineering, North China University of Technology, Beijing 100144, China

e-mail: zhanglifeng@ncut.edu.cn

chemical activity, rare earth elements readily react with refractory materials during the steelmaking process. Yu et al. [6] investigated the interfacial reaction between rare earth steel and different kinds of refractory materials. It was found that there are great differences in the reaction mechanisms between various refractory materials and rare earth steel. SiO₂ refractory can react with rare earth steel to form a glass phase with a low melting point, which can accelerate the corrosion of refractory materials. For the reaction between Al₂O₃ refractory and rare earth steel, a silicate phase with a high melting point was observed. This phase exhibits a weak adsorption force for the inclusions. However, the low melting point glass phase formed by the reaction between silica-aluminum refractory and molten steel exhibits stronger adsorption forces compared to the inclusion. Wang et al. [7, 8] reported that the rare earth element lanthanum in the steel first reacts with Si-Mn-Al-O inclusions and then reacts with the refractory material. Sun et al. [9] investigated the effect of cerium content on the interaction between stainless steel and Al₂O₃ refractory. The results indicate that during the initial reaction, the Al₂O₃ inclusion in the steel was reduced by dissolved cerium, forming Ce-Al-O composite inclusion. However, due to the reaction between the refractory materials and steel, the cerium content in the steel continuously decreases, and the Ce-Al-O composite inclusions are modified to aluminum-rich silicate inclusions. Zhang et al. [10] observed a rare earth oxide layer at the interface between cerium-bearing steel and Al₂O₃-MgO refractory. This reaction layer inhibits the diffusion of molten steel into the refractory and increases the contact angle. However, previous studies on the reaction between rare earth-bearing steel and refractory materials have mostly focused on quiescent conditions, with few studies conducted under dynamic conditions. In the current study, author investigate the interfacial reaction between molten steel and the MgO-C refractory under rotational conditions.

Laboratory Experiment and Analysis

Commercial stainless steel with the composition shown in Table 1 was used as the base material in the experiment. MgO-C refractory rods (Ø 50 × H 150 mm) were cut from commercial MgO-C refractory bricks. The chemical compositions are shown in Table 2. The experimental conditions are shown in Table 3. For the dynamic experiment, the rotational speed was 120 rpm. For the lanthanum-bearing steel, the addition of lanthanum was 1000 ppm.

The experimental setup and procedure are depicted in Figs. 1 and 2. A silicon molybdenum resistance furnace was used to investigate the dynamic interaction

Table 1 Chemical composition of steel (wt.%)

Elemental	C	Mn	Si	Cr	S	T.Al	Ti	N	Ca, Mg
wt.%	0.021	1.08	0.547	11.66	0.0009	0.026	0.117	0.017	< 0.0005

Table 2 Chemical composition of refractory (wt.%)

Composition	MgO	C	Al	SiO ₂	CaO	Fe ₂ O ₃	Others
wt.%	77.6	10	4.91	4.41	2.09	0.6	≤ 0.39

Table 3 Experimental condition

Sample	Lanthanum addition (ppm)	Rotational speed (rpm)
M0-0	0	0
M0-120	0	120
M1000-0	1000	0
M1000-120	1000	120

between MgO-C refractory and molten steel. The experimental devices are shown in Fig. 1. 700 g of steel were placed into a crucible made of alumina castable. Argon was then pumped into the resistance furnace, heating the crucible containing steel to 1600 °C. After the steel melted, it was kept at a temperature of 1600 °C for 5 min to ensure uniform composition. Lanthanum alloy was added to the liquid steel, and after 5 min, the MgO-C refractory rod was inserted into the liquid steel. The rod was rotated using an electrical machinery device, as shown in Figs. 1 and 2.

The compositions of the refractory were determined using X-ray fluorescence (XRF) analysis. The steel-refractory boundary was cut to obtain a horizontal cross-section and then polished. The boundary layer was investigated to analyze its morphology, composition, and thickness using scanning electron microscopy (SEM) with energy-dispersive X-ray spectrometry (EDS).

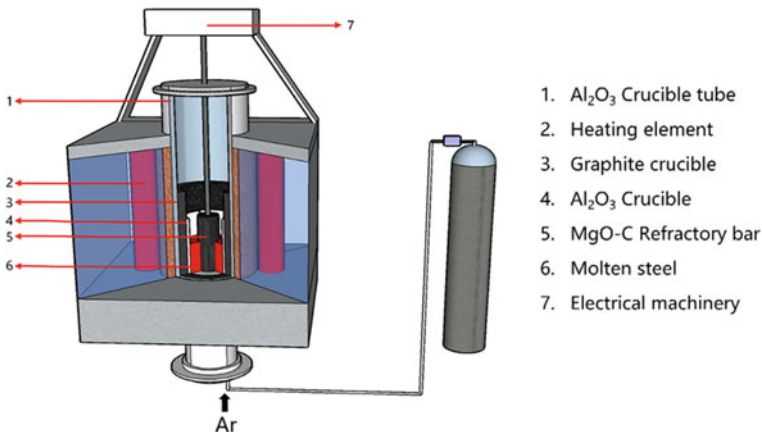


Fig. 1 Schematic of experimental setup

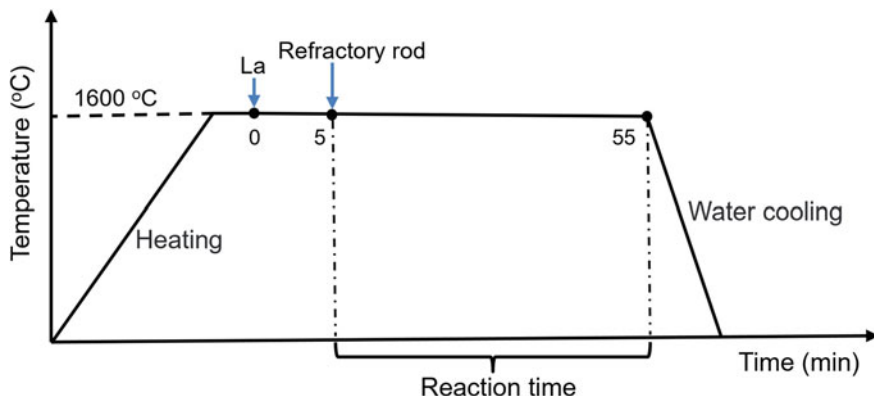
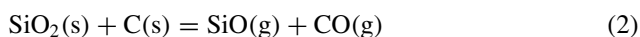


Fig. 2 Schematic of procedure in the present study

Interfacial Reaction Between the Steel and the MgO-C Refractory

Figure 3 displays the typical morphology and elemental diagrams of MgO-C refractories before and after the reaction of refractories with molten steel under quiescent conditions. A significant amount of $\text{CaO}(-\text{SiO}_2)$ impurities were observed at the boundary of MgO particles, as shown in Fig. 3a. However, after the reaction between the refractory and molten steel, the $\text{CaO}(-\text{SiO}_2)$ impurity disappears and creates voids, as shown in Fig. 3b. According to the report of Brabie's [11], the reaction equation is presented as follows:



At high temperatures, the Ca vapor and SiO vapor generated by reaction Eqs. (1) and (2), diffuse through the pores of MgO particles to reach the interface between the refractory materials and steel.

The morphology and elemental mapping of the typical interface between the quiescent steel without lanthanum and the refractory are shown in Fig. 4. Figure 4b is an enlarged view of Square 1 in Fig. 4a. A dense MgO reaction layer with a thickness of 50 μm was observed at the interface between the steel and refractory. Some molten steel penetrated the refractory, and a dense layer was formed, separating the refractory from the molten steel. The penetration of molten steel into the MgO-C refractory was inhibited, as shown in Fig. 4a. The formation mechanism of the MgO layer has been widely recognized. It has been widely reported that the primary reaction occurring at high temperatures is the reduction of MgO by C within the refractory. The reaction equation is shown in Eq. (3). [12–14] Brabie and Liu et al. [11, 15–17] reported

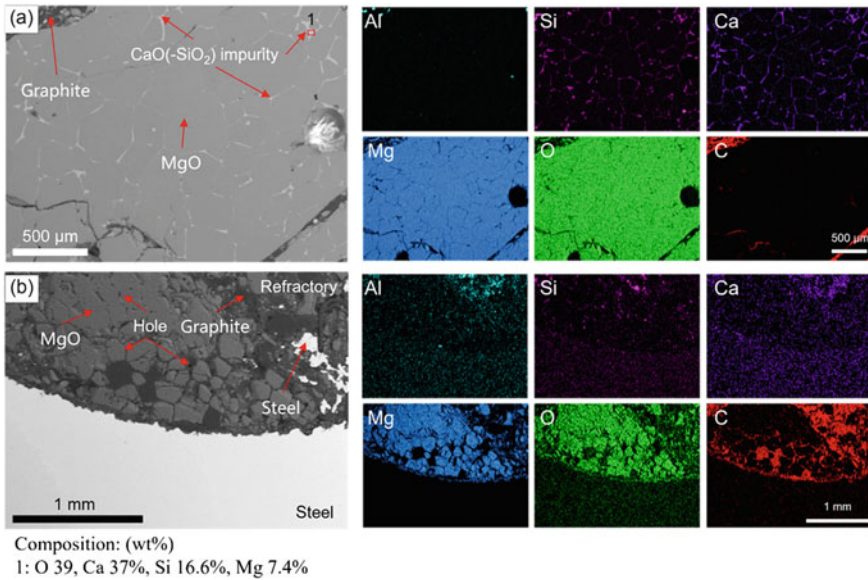


Fig. 3 Morphology and element mapping of the MgO-C refractory under quiescent conditions. **a** Before reaction; **b** after reaction

that at high temperatures, the magnesia-carbon refractory undergoes a reaction to produce magnesium vapor and CO, as shown in Eq. (3). The magnesium vapor can then diffuse towards the interface of the molten steel through the pores of the MgO-C refractory, driven by the concentration gradient. At the interface, the magnesium vapor is oxidized to form MgO, which then condenses and creates a layer of MgO.



Figure 5 shows the morphology and elemental mapping of the interface between the lanthanum-free steel and the refractory under stirring conditions. Figure. 5b, c were the enlarged views of Square 1 and Square 2, respectively, in Fig. 5a. A dense MgO reaction layer with a thickness of 25 μm was observed at the interface between the steel and refractory. However, the layer was found to be non-continuous and broken at certain locations, as shown in Fig. 5a, b. It can be seen that the molten steel penetrated into the refractory through the crack in the MgO layer, as shown in Fig. 5b, c. Under stirring conditions, the impact force of molten steel on the MgO reaction layer was greater than that under quiescent conditions, thereby causing cracks in the reaction layer. In addition, the stirring induced the MgO particles to become dislodged from the MgO-C refractory and enter the molten steel, as shown in Fig. 6. Figure. 6b is an enlarged view of Square 1 in Fig. 6a.

Figure 7 shows the morphology and elemental mapping of the interface between the lanthanum-bearing steel and the MgO-C refractory under quiescent conditions.

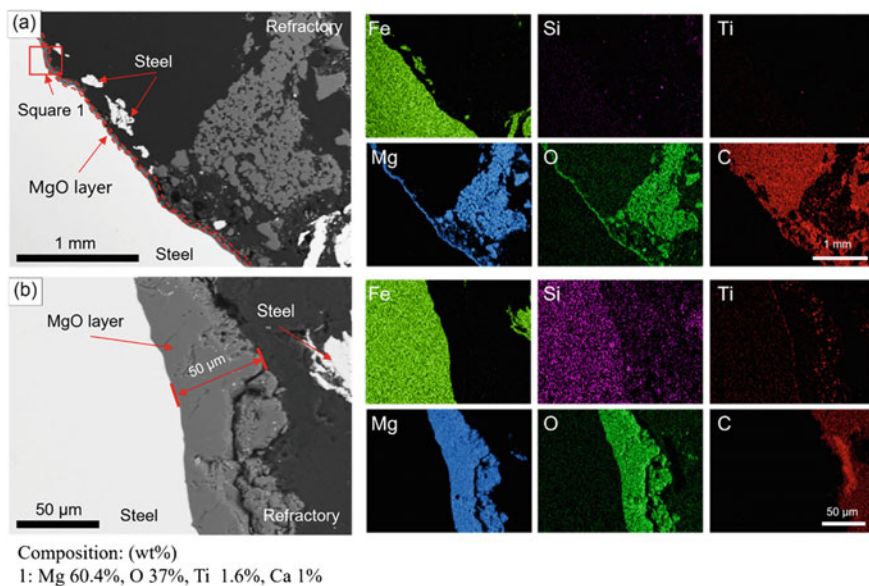


Fig. 4 Morphology and elemental mapping of the typical interface between the quiescent steel without lanthanum and the MgO-C refractory. **b** is an enlarged view of Square 1 in **(a)**

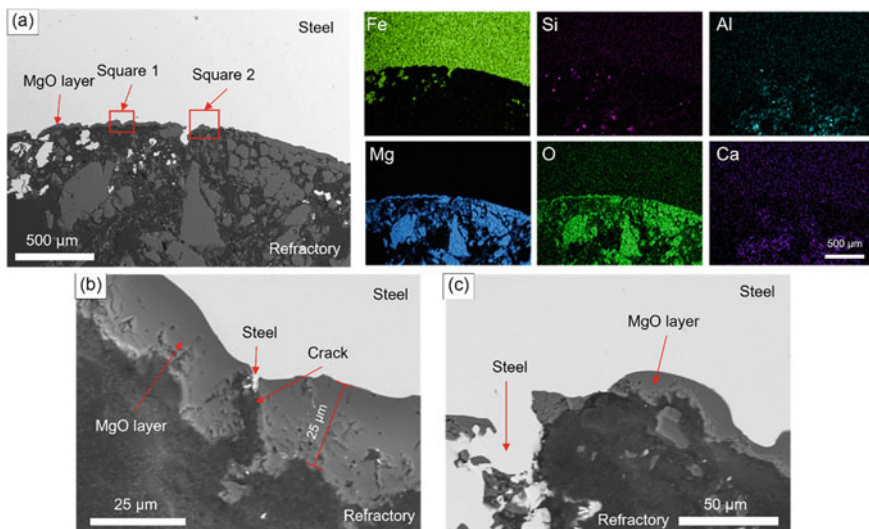


Fig. 5 Morphology and elemental mapping of the interface between the steel without lanthanum and the MgO-C refractory under stirring conditions. **b** is an enlarged view of Square 1 in **(a)**; **c** is an enlarged view of Square 2 in **(a)**

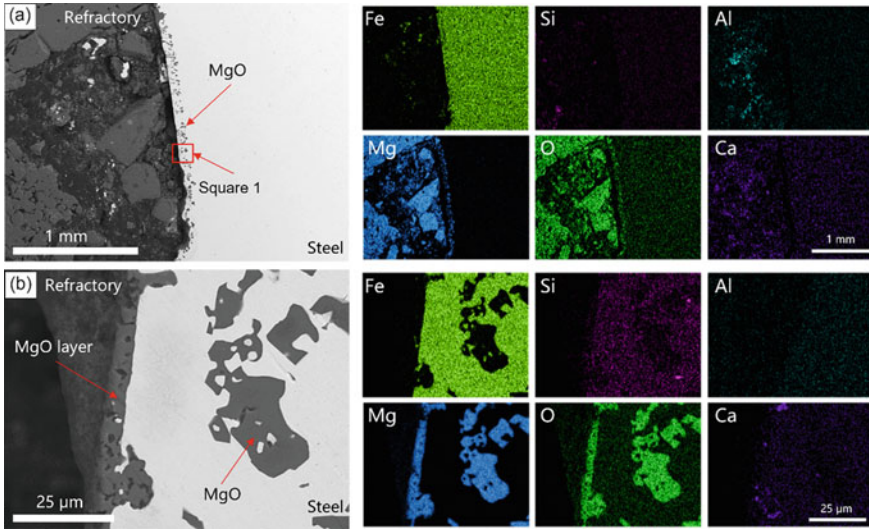


Fig. 6 Morphology and elemental mapping of the interface between the steel without lanthanum and the refractory under stirring conditions. **b** is an enlarged view of Square 1 in (a)

A double-layer structure was observed, with a MgO layer close to the refractory side and a La₂O₃ layer close to the steel side, as shown in Fig. 7a. The La₂O₃ layer was only 3–5 μm thick, but it was dense and continuous. The La₂O₃ layer forms as a result of the reaction between dissolved lanthanum in the steel and MgO at the interface between the molten steel and refractory. The reaction equation is presented as follows:

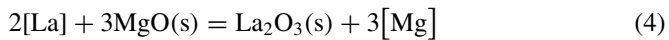
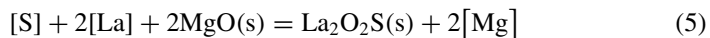


Figure 8 shows the morphology and elemental mapping of the interface between the lanthanum-bearing steel and the MgO-C refractory under stirring conditions. A MgO reaction layer was formed at the interface between the steel and refractory, as shown in Fig. 8a. Additionally, a layer containing La was detected outside of the MgO reaction layer. The La-containing reaction layer was primarily composed of La₂O₃ and La₂O₂S, as shown in Fig. 8b. The La₂O₂S layer forms as a result of the reaction between dissolved lanthanum and sulfur in the steel, as well as MgO at the interface between the molten steel and refractory. The reaction equation is presented as follows:



In addition, a few LaAlO₃ particles were embedded within the MgO reaction layer, as shown in Fig. 9. Under stirring conditions, the MgO particles formed were drawn into the steel, as shown in Fig. 6a. Subsequently, the MgO particles in the

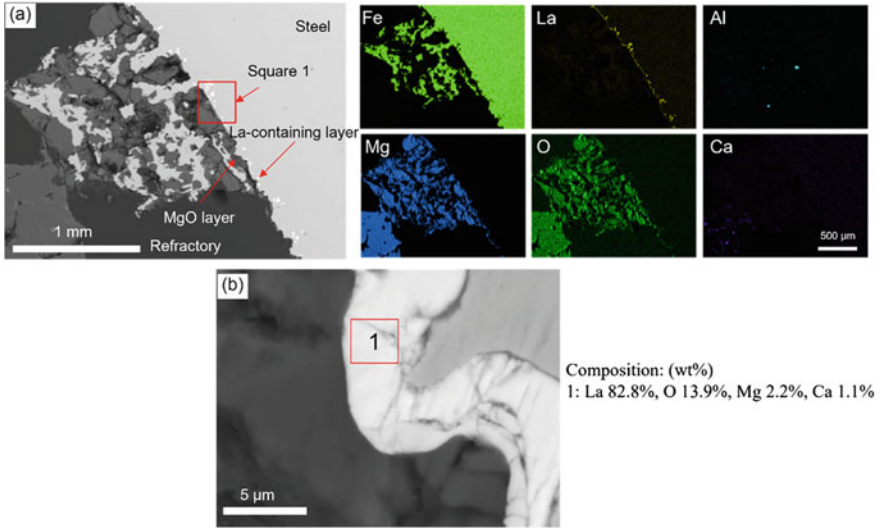


Fig. 7 Morphology and elemental mapping of the interface between the lanthanum-bearing steel and the MgO-C refractory under quiescent conditions. **b** is an enlarged view of Square 1 in **(a)**

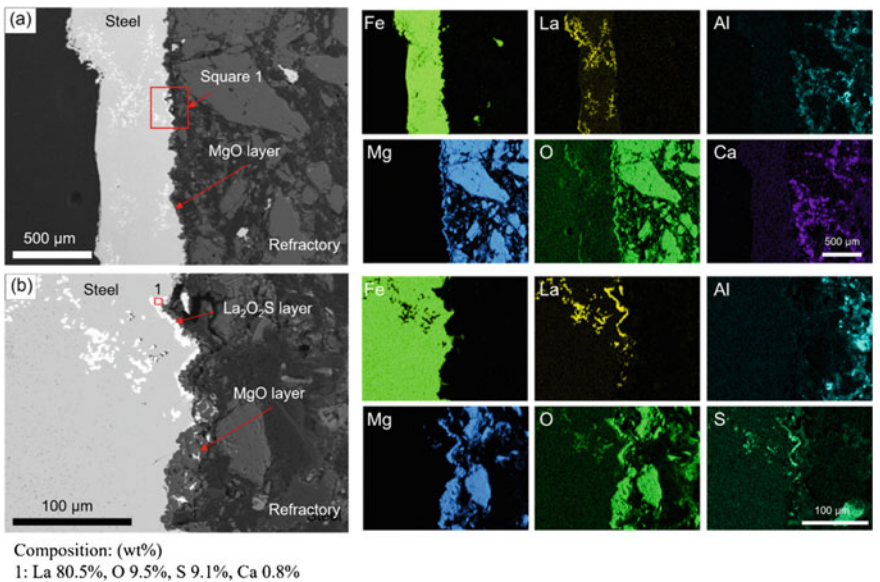


Fig. 8 Morphology and elemental mapping of the interface between the lanthanum-bearing steel and the MgO-C refractory under stirring conditions. **b** is an enlarged view of Square 1 in **(a)**

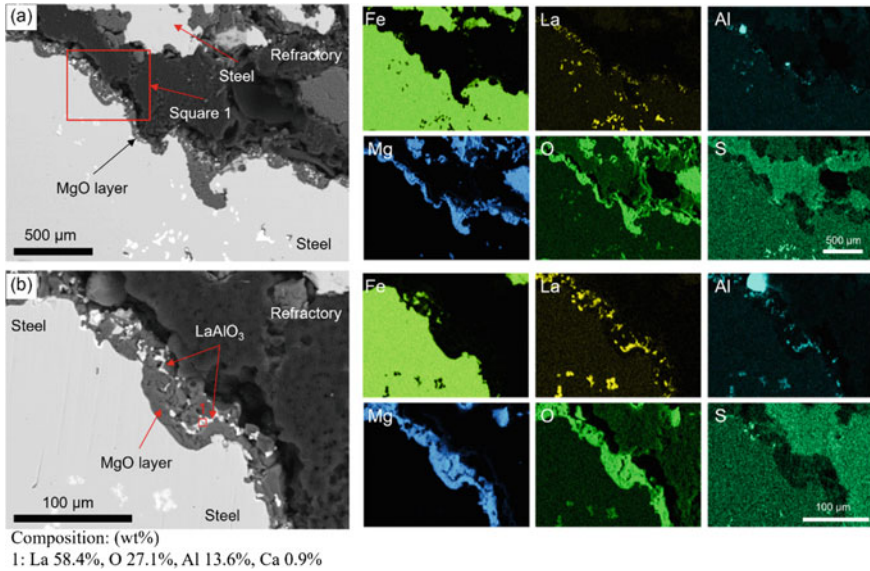


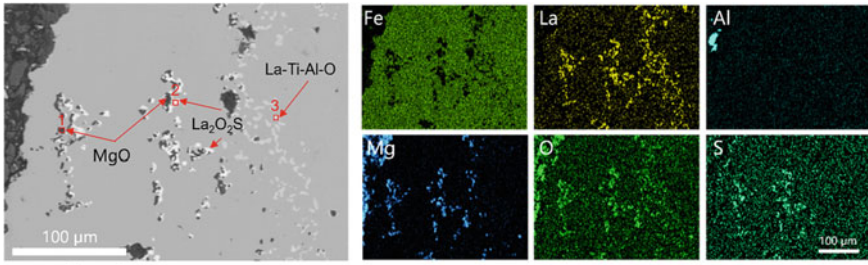
Fig. 9 Morphology and elemental mapping of the reaction layer at the interface between the lanthanum-bearing steel and the MgO-C refractory under stirring conditions. **b** is an enlarged view of Square 1 in **(a)**

steel precipitate to form a reaction layer. At the same time, the lanthanum oxides were formed at the MgO reaction layer, as shown in Fig. 9b. The lanthanum oxides embedded in the MgO layer react with aluminum in the MgO-C refractory to form LaAlO₃, as shown in Fig. 9b.

For the interfacial reaction between lanthanum-bearing steel and refractory under stirring conditions, numerous foreign inclusions from the refractory fall off into the steel, as shown in Fig. 10. The MgO particles in the steel initially react with dissolved lanthanum and sulfur to form La₂O₂S and La₂O₃ inclusions, as shown in Eqs. (4) and (5). Then, the lanthanum-containing inclusions react with dissolved titanium and aluminum in the steel to form La-Ti-Al-O inclusions, as shown in Fig. 10. The transformation of inclusion is as follows: MgO → La₂O₂S → La-Ti-Al-O.

Interaction Mechanism

The schematic diagram of the interface reactions between the MgO-C refractory and the molten steel is shown in Fig. 11. Under quiescent conditions, a MgO reaction layer forms at the interface between molten steel and MgO-C refractory. After adding lanthanum to the steel, the dissolved lanthanum diffuses to the interface and reacts with MgO, resulting in the formation of a reaction layer that contains lanthanum. Under stirring conditions, the reaction layer was non-continuous and fragmented.



Composition: (wt%)
 1: Mg 62.6%, O 37.4%. 2: La 79.2%, S 10.6%, O 8.9%, Mg 1.3%. 3: La 65.2%, O 20.6%, Ti 11.6%, Al 2.6%

Fig. 10 Morphology and elemental mapping of the interface between the lanthanum-bearing steel and the MgO-C refractory under stirring conditions

The stirring induced the dislodgement of MgO particles from the MgO-C refractory into the molten steel. For the lanthanum-bearing steel, the MgO particles from the refractory are transformed into $\text{La}_2\text{O}_2\text{S}$ and La-Al-Ti-O inclusions.

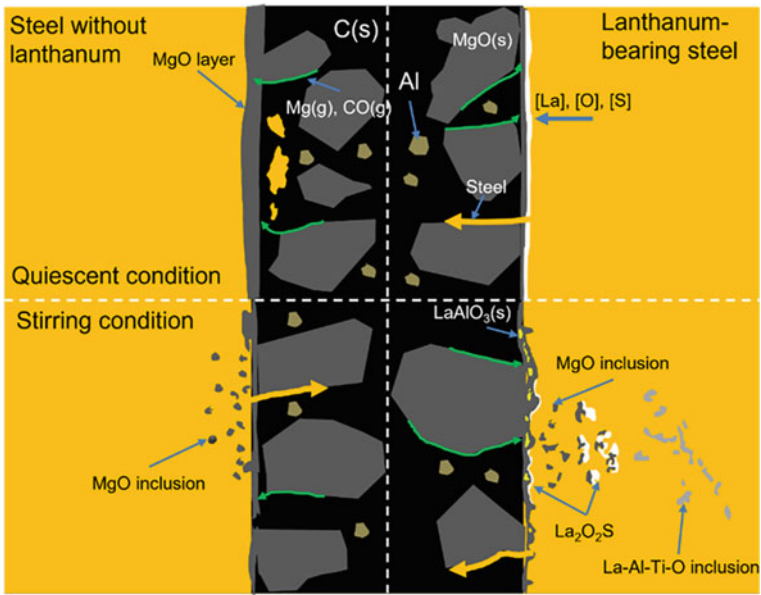


Fig. 11 Schematic of the interaction between steel and refractory

Conclusions

- (1) For the reaction between steel without lanthanum and MgO-C refractory, a dense 50 μm thick MgO reaction layer was observed under quiescent conditions. However, under stirring conditions, the thickness of the MgO reaction layer was only 25 μm . Additionally, the layer was non-continuous and broken at certain locations. In addition, the molten steel will penetrate the refractory through the crack in the MgO reaction layer.
- (2) After the reaction between lanthanum-bearing steel and MgO-C refractory under quiescent conditions, a double-layer structure is formed. The structure consists of a MgO layer close to the refractory side and a La_2O_3 layer close to the steel side. The La_2O_3 layer can inhibit the penetration of molten steel into refractory materials. Under stirring conditions, a layer of La_2O_3 - $\text{La}_2\text{O}_2\text{S}$ was formed, with a few LaAlO_3 particles embedded within the MgO reaction layer.
- (3) Under stirring conditions, the stirring induced the MgO particles to detach from the refractory lining and enter the molten steel. For the lanthanum-bearing steel, the MgO particles from the refractory will react with dissolved lanthanum, aluminum, and titanium in the steel, resulting in the transformation of inclusions as follows: $\text{MgO} \rightarrow \text{La}_2\text{O}_2\text{S} \rightarrow \text{La-Ti-Al-O}$.

Acknowledgements The authors are grateful for support from the National Natural Science Foundation of China (Grant No. U22A20171, No. 52104343), the Natural Science Foundation of Hebei Province (Grant No. E2021203222), and the High Steel Center (HSC) at Yanshan University and the High Steel Center (HSC) at North China University of Technology, China.

References

1. Huang A, Wang Y, Gu H, Zou Y (2018) Dynamic interaction of refractory and molten steel: effect of alumina-magnesia castables on alloy steel cleanliness. *Ceram Int* 44(18):22146–22153
2. Wang L (2004) Application prospects and behavior of RE in new generation high strength steels with superior toughness. *J Chinese Rare Earths* 22(1):48–54
3. Yin N, Jing CL, Li HB, Chu RS, Chen B (2019) Effect of rare earth elements on the inclusion behavior in low alloy structural steel. *Mater Sci Forum* 944(1):364–372
4. Zhang J, Zhang L (2020) Application and research progress of rare earth elements in stainless steels. *J Yanshan Univ* 44(3):268–273
5. Liang Y, Shi Z, Li G, Zhang R, Li M (2019) Effects of rare earth modification on microstructure refinement and mechanical properties of Al-2 wt%Fe alloys. *Mater Res Express* 6(10):106504
6. Yu Z, Zhao W, Xie Y, Yu Q (1983) Investigation on the reaction of refractories with rare earth metals bearing steels and nozzle blockage. *Iron and Steel* 19(19):3
7. Wang H, Xiong L, Zhang L, Wang Y, Shu Y, Zhou Y (2017) Investigation of RE-O-S-As inclusions in high carbon steels. *Metall Mater Trans B* 48(6):2849–2858
8. Wang H, Jiang S, Yu P, Sun L, Wang Y (2020) Effect of steel-refractory reactions on removal of arsenic from molten steel with lanthanum additions. *ISIJ Int* 60(11):2316–2324
9. Kwon SK, Park JS, Park JH (2015) Influence of refractory-steel interfacial reaction on the formation behavior of inclusions in ce-containing stainless steel. *ISIJ Int* 55(12):2589–2596

10. Zhang L, Cheng L, Ren Y, Zhang J (2020) Effect of cerium on the wettability between 304 stainless steel and MgO–Al₂O₃-based lining refractory. *Ceram Int* 46(10):15674–15685
11. Voicu B (1997) A study on the mechanism of reaction between refractory materials and aluminium deoxidised molten steel. *Steel Res* 68(2):54–60
12. Li X, Rigaud M, Palco S (1995) Oxidation kinetics of graphite phase in magnesia-carbon refractories. *J Am Ceram Soc* 78(4):965–971
13. Volkova O, Scheller PR, Lychatz B (2014) Kinetics and thermodynamics of carbon isothermal and non-isothermal oxidation in MgO-C refractory with different air flow. *Metall and Mater Trans B* 45(5):1782–1792
14. Wang L, Zhu H, Zhao J, Song M, Xue Z (2022) Steel/refractory/slag interfacial reaction and its effect on inclusions in high-Mn high-Al steel. *Ceram Int* 48(1):1090–1097
15. Chen L, Chen W, Hu Y, Chen Z, Xu Y, Yan W (2016) Effect of Al antioxidant in MgO–C refractory on the formation of Al₂O₃-rich inclusions in high-carbon steel for saw wire under vacuum conditions. *Ironmaking Steelmaking* 45(3):272–279
16. Jansson S, Brabie V, Jönsson P (2006) Magnesia–carbon refractory dissolution in Al killed low carbon steel. *Ironmaking Steelmaking* 33(5):389–397
17. Watanabe A, Takahashi H, Nakatani F (2010) Mechanism of dense magnesia layer formation near the surface of magnesia-carbon brick. *J Am Ceram Soc* 69(9):213–214